An SCADTV Nonconvex Regularization Approach for Magnetic Resonance Imaging

Zhijun Luo, Zhibin Zhu, and Benxin Zhang

Abstract—**In this paper, we propose a non-convex regularization magnetic resonance imaging (MRI) reconstruction model via the smoothly clipped absolute deviation (SCAD) penalty function, which can effectively improve the fitting performance and prevent systematic underestimation compared with the classical total variation (TV) regularization. Then, we choose the alternating direction method of multipliers (ADMM) algorithm to solve the non-convex regularization model. The experiment results show that the efficiency of the proposed model and algorithm in comparison with some other typical methods.**

Index Terms—**MRI reconstruction, TV regularization, SCAD penalty function, ADMM.**

1. Introduction

MAGNETIC resonance imaging (MRI) has been widely used in the medical field due to its non-radiation and non-ionizing nature, as well as its powerful capability in providing rich anatomical and functional information. However, several constraints, such as nuclear relaxation times, signal to noise, power absorption, and so on, make MRI be a time-consuming procedure. Moreover, the longer the MRI, the more uncomfortable the patient will be, and the higher the possibility of artifacts will increase. Therefore, to cut back the acquisition time of MRI, a lot of techniques (such as multi coils [1]-[3], parallel imaging [4]-[5], and sparse sampling [7]-[13], etc) have been developed. Among them, compressed sensing technology is particularly prominent [6]-[7], because it is easier to reconstruct the accurate signal than the traditional Shannon-Nyquist sampling criterion when the signal is sparse and satisfies certain assumptions. Compressed sensing has become the focus of the MRI community since the invention of the pioneering work compression sensing MRI (CS-MRI) [14].

Manuscript received November 06, 2020; revised July 19, 2021. This work is supported in part by the National Natural Science Foundation of China under Grants 11901137 and 61967004, in part by the China Postdoctoral Science Foundation under Grant 2020M682959, in part by the Natural Science Foundation of Guangxi province under Grant 2018GXNSFBA281023, in part by Scientific Research Fund of Hunan Provincial Education Department 20A273, and in part by Research Fund of Mathematics Discipline of Hunan University of Humanities, Science and Technology 2020SXJJ01.

Zhijun, Luo is a PHD candidate in the School of Electronic Engineering and Automation and Guangxi Key Laboratory of Automatic Detecting Technology and Instruments, Guilin University of Electronic Technology, Guilin, 541004, P. R. China, and an associate Professor in the School of Mathematics and Finance, Hunan University of Humanities, Science and Technology, Loudi, 417000, P. R. China e-mail: ldlzj123@163.com.

Zhibin, Zhu is a Professor in the School of Mathematics and Computing Science and Guangxi Colleges and Universities Key Laboratory of Data Analysis and Computation, Guilin University of Electronic Technology, Guilin, 541004, P. R. China. Corresponding author, e-mail: optimization_zhu@163.com.

Benxin, Zhang is an associate Professor in the School of Electronic Engineering and Automation and Guangxi Key Laboratory of Automatic Detecting Technology and Instruments, Guilin University of Electronic Technology, Guilin, 541004, P. R. China. e-mail: bxzhang@guet.edu.cn.

In the MRI field, researchers commonly formulate the data acquisition as

$$\mathbf{y} = \underbrace{\mathbf{RF}}_{\mathbf{A}}\mathbf{x} + \varepsilon = \mathbf{Ax} + \varepsilon, \tag{1.1}$$

where $\mathbf{x}$ and ε are the desired MR image and noise/disturbance, respectively; $\mathbf{R}$ and $\mathbf{F}$ denote the undersampling operator and the Fourier operator, respectively; $\mathbf{y}$ represents the undersampled $k-$ space measurement, and its scale is much smaller than that of $\mathbf{x}$. MR image reconstruction aims to recover $\mathbf{x}$ from $\mathbf{y}$. Compressed sensing based reconstruction techniques commonly model the reconstruction as

$$\min_{\mathbf{x}} \lambda\|\mathbf{x}\|_{\mathrm{TV}} + \frac{1}{2}\|\mathbf{y} - \mathbf{Ax}\|_2^2, \tag{1.2}$$

where $\|\mathbf{x}\|_{\mathrm{TV}} = \|\mathbf{Dx}\|_1$ ($\mathbf{D}$ is finite difference operator), $\lambda > 0$ is the regularization parameter. Under some conditions of A [7], the classical TV regularization is formulated as a convex optimization problem involving an ℓ_1-norm regularization. The minimizer of cost function is unique. However, the use of ℓ_1-norm regularization suffers from two limitations [10], [15]: 1) the estimation for large coefficients may be biased, 2) it is unable to recover a signal by the least measurements. Therefore, many non-convex regularizations have been developed for dealing with these issues [16]-[22]. For instance, the ℓ_p-norm regularization was studied in [16], [20], and its significantly better recovery performance than ℓ_1-regularization was verified. Inspired by the Moreau envelope and minimax-concave penalty, a nonseparable non-convex TV regularization was proposed in [21] and extended in [23], [24]. Smoothly clipped absolute deviation (SCAD) is another non-convex penalty function, which was originally proposed by Fan and Li [25]. Mehranian et al. [26] have studied the SCAD norm for CS-MRI using an augmented Lagrangian method. In view of the good properties of SCAD penalty such as sparsity and oracle, in this paper, we use SCAD norm to construct a non-convex regularization model for MRI reconstruction.

Fast imaging algorithm is another focus of MR image reconstruction. In recent decades, a large number of fast optimization algorithms have been developed using the structure and regularizers of the system model in MRI, such as segmentation algorithms (SA) [27], augmented lagrangian methods (ALM) [28]-[29], primal-dual methods [31]-[32], splitting methods [33]-[35], the fast iterative soft thresholding algorithms (FISTA) [36]-[39], alternating direction method of multipliers (ADMM) algorithms [40]-[46] etc. For more detailed discussion, can see [47]. In this paper, we will solve the proposed model by ADMM iteration, which is simple in structure similar to the ALM and equivalent to some other splitting algorithms under certain conditions [48].

The main contribution of this article can be summarized as following: 1) We construct a more accurate MRI reconstruction non-convex model via SCAD penalty function. The most important feature of the new model has good properties of selecting variables and estimating coefficients at the same time. That is, the SCAD non-convex regularization improves the performance of TV regularization technique. 2) To solve the proposed model, we introduce the ADMM method which can successfully solve non-convex optimization problems [50]. 3) In order to evaluate the performance, a number of experiments are carried out with different sampling masks and MR data sets.

The rest of this paper is organized as follows. Section 2 introduces the non-convex MRI reconstruction model via SCAD penalty function. In Section 3, the fast algorithm ADMM is presented. Section 4 contains experimental results. At last, some conclusions are made in Section 5.

2. Non-convex MRI reconstruction model

In this section, we recalled the definition of smoothly clipped absolute deviation (SCAD) function and showed its properties, then defined SCADTV regularization using the penalty function. Finally, we proposed a non-convex regularization model for MRI reconstruction.

Definition 2.1. *[51] The SCAD function $\phi : \mathbb{R} \to \mathbb{R}$ is defined as*

$$\phi_\gamma(x) = \begin{cases} |x|, & |x| < \gamma_1, \\ \frac{2\gamma_2|x| - x^2 - \gamma_1^2}{2(\gamma_2 - \gamma_1)}, & \gamma_1 \le |x| < \gamma_2, \\ \frac{\gamma_1 + \gamma_2}{2}, & |x| \ge \gamma_2, \end{cases} \tag{2.3}$$

for some $\gamma_2 > \gamma_1 > 0$, where γ_1 and γ_2 are threshold parameters, $\gamma := (\gamma_1, \gamma_2)$.

From the definition of SCAD function, we consider another function $\psi_\lambda(x)$ as following,

$$\psi_\gamma(x) := |x| - \phi_\gamma(x) = \begin{cases} 0, & |x| < \gamma_1, \\ \frac{x^2 - 2\gamma_1|x| + \gamma_1^2}{2(\gamma_2 - \gamma_1)}, & \gamma_1 \le |x| < \gamma_2, \\ |x| - \frac{\gamma_1 + \gamma_2}{2}, & |x| \ge \gamma_2. \end{cases} \tag{2.4}$$

It's easy to see that the function of $\psi_\gamma(x)$ is convex, differentiable and satisfies $0 < \psi_\gamma(x) < |x|$. The graph of $\psi_\gamma(x)$ is illustrated in Fig. 1(a). Then, the SCAD function can be written as $\phi_\gamma(x) = |x| - \psi_\gamma(x)$.

Proximity operator plays a key role in developing highly-efficient first-order algorithms which scale well to high-dimensional problems. In [25], Fan and Li suggested $\gamma_2 = a\gamma_1 \quad (a > 2, a \approx 3.7)$, the corresponding proximity operator of (2.4) is

$$\begin{aligned} &\mathrm{prox}_{\phi_\gamma,\eta}(t) = \arg\min_x \{\phi_\gamma(x) + \tfrac{\eta}{2}(x-t)^2\} \\ &= \begin{cases} \mathrm{sign}(t)\max\{|t| - \gamma_1, 0\}, & |t| \le 2\gamma_1, \\ \frac{(a-1)t - \mathrm{sign}(t)a\gamma_1}{a-2}, & 2\gamma_1 < |t| \le a\gamma_1, \\ t, & |t| > a\gamma_1, \end{cases} \end{aligned} \tag{2.5}$$

and its graph is shown in in Fig. 1(b).

For MRI model, we define the corresponding multivariate functions $\phi_\gamma(x)$ as follows

$$\Phi_\gamma(\mathbf{v}) = \sum_{i=1}^{\mathbb{N}} \phi_\gamma(v_i), \quad \mathbf{v} \in \mathbb{R}^{\mathbb{N}}.$$

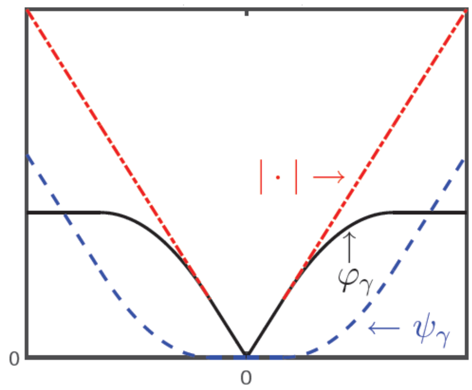

(a) SCAD function

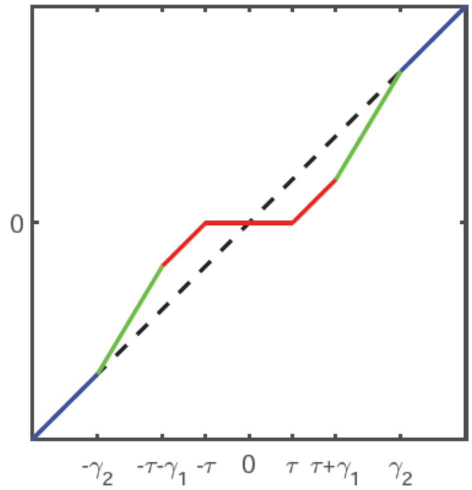

(b) SCAD proximity operator

Fig. 1. SCAD function and its proximity operator

The extension function of $\psi_\gamma(x)$ is given by

$$\Psi_\gamma(\mathbf{v}) = \sum_{i=1}^{\mathbb{N}} \psi_\gamma(v_i), \quad \mathbf{v} \in \mathbb{R}^{\mathbb{N}},$$

then, for all $\mathbf{v} \in \mathbb{R}^{\mathbb{N}}$, $\Phi_\gamma(\mathbf{v}) = \|\mathbf{v}\|_1 - \Psi_\gamma(\mathbf{v})$. Now, we consider replacing $\mathbf{v}$ with gradient $\mathbf{Dx}$ in above-mentioned equation, which leads to our definition of SCADTV as follows.

Definition 2.2. *The SCAD penalty function of non-convex TV regularizer: $\|\mathbf{x}\|_{SCADTV} : \mathbb{R}^{\mathbb{N}} \to \mathbb{R}$*

$$\|\mathbf{x}\|_{SCADTV} = \Phi_\gamma(\mathbf{Dx}) = \|\mathbf{Dx}\|_1 - \Psi_\gamma(\mathbf{Dx}), \tag{2.6}$$

where $\mathbf{D}$ is the first-order difference matrix.

Now, we consider the following formulation for magnetic resonance imaging (MRI)

$$\min_{\mathbf{x}} \lambda\|\mathbf{x}\|_{\mathrm{SCADTV}} + \frac{1}{2}\|\mathbf{y} - \mathbf{Ax}\|_2^2 \tag{2.7}$$

where $\|\mathbf{x}\|_{\mathrm{SCADTV}}$ is given by (2.6), $\lambda > 0$ is called regularization parameter. For $\Phi_\gamma(\cdot)$ is non-convex, the model (2.7) is non-convex model.

3. Proposed algorithm

We rewrite the problem (2.7) as following:

$$\min_{\mathbf{x}} \lambda\Phi_\gamma(\mathbf{Dx}) + \frac{1}{2}\|\mathbf{y} - \mathbf{Ax}\|_2^2. \tag{3.8}$$

We define the auxiliary variable $\mathbf{z} = \mathbf{Dx}$, the model (3.8) can be expressed as an equality-constrained optimization problem as

$$\min_{\mathbf{x}} \lambda\Phi_\gamma(\mathbf{z}) + \frac{1}{2}\|\mathbf{y} - \mathbf{Ax}\|_2^2, \text{ s.t } \mathbf{z} = \mathbf{Dx}. \tag{3.9}$$

Hence, the augmented Lagrangian function of (3.9) can be written as

$$\begin{aligned}&\mathcal{L}(\mathbf{x}, \mathbf{z}, \mathbf{w}) \\ &= \lambda\Phi_\gamma(\mathbf{z}) + \tfrac{1}{2}\|\mathbf{y} - \mathbf{Ax}\|_2^2 - \mathbf{w^T}(z - \mathbf{Dx}) + \tfrac{\rho}{2}\|\mathbf{z} - \mathbf{Dx}\|_2^2,\end{aligned}$$

where $\Phi_\gamma(\mathbf{z}) = \|\mathbf{z}\|_1 - \Psi_\gamma(\mathbf{z})$, $\mathbf{w}$ is a Lagrange multiplier and $\rho > 0$ is a penalty parameter. According to the standard ADMM, the iterative scheme of the problem (3.9) can be expressed as solving the following sub-problems

$$\begin{cases} \mathbf{x}^{k+1} = \operatorname{argmin} \mathcal{L}(\mathbf{x}, \mathbf{z^k}, \mathbf{w^k}) \\ = \operatorname{argmin}_{\mathbf{x}}\{\tfrac{1}{2}\|\mathbf{y} - \mathbf{Ax}\|_2^2 + \mathbf{w}^{kT}\mathbf{Dx} + \tfrac{\rho}{2}\|\mathbf{z^k} - \mathbf{Dx}\|_2^2\}, \\ \mathbf{z}^{k+1} = \operatorname{argmin} \mathcal{L}(\mathbf{x^{k+1}}, \mathbf{z}, \mathbf{w^k}) \\ = \operatorname{argmin}_{\mathbf{z}}\{\lambda\Phi_\gamma(\mathbf{z}) - \mathbf{w^{kT}z} + \tfrac{\rho}{2}\|\mathbf{z} - \mathbf{Dx^{k+1}}\|_2^2\}, \\ \mathbf{w}^{k+1} = \mathbf{w}^k - \rho(\mathbf{Dx^{k+1}} - \mathbf{z}^{k+1}). \end{cases}$$

Now, we show how to solve the subproblems. For $\mathbf{x}$-minimization step, the optimization subproblem for $\mathbf{x}^{k+1}$ can be solved via the first-order optimality optimality conditions,

$$\mathbf{x^{k+1}} = (\rho\mathbf{D^TD} + \mathbf{A^TA})^{-1}\widehat{\mathbf{H}}_\mathbf{k}, \tag{3.10}$$

where $\widehat{\mathbf{H}}_\mathbf{k} = \rho\mathbf{D^Tz^k} + \mathbf{A^Ty} - \mathbf{D^Tw^k}$. In the field of MRI, $\mathbf{A} = \mathbf{RF}$ ($\mathbf{F}$ is the Fourier operator such that $\mathbf{F} = \mathbf{F^{-1}}$), and $\mathbf{D^TD}$ is circulant matrix which can be diagonalized via Fourier transform. For simplicity, we can get the optimal solution of $\mathbf{x^{k+1}}$ through two Fourier transforms.

For $\mathbf{z}$-minimization sub-problem:

$$\begin{aligned}\mathbf{z}^{k+1} &= \min_{\mathbf{z}}\{\lambda\Phi_\gamma(\mathbf{z}) - \lambda\mathbf{w^{kT}z} + \frac{\lambda\rho}{2}\|\mathbf{z} - \mathbf{Dx^{k+1}}\|_2^2\} \\ &= \min_{\mathbf{z}}\{\Phi_\gamma(\mathbf{z}) + \frac{\rho}{2}\|\mathbf{z} - (\mathbf{Dx^{k+1}} + \frac{\mathbf{w^k}}{\rho})\|_2^2\}\end{aligned} \tag{3.11}$$

Follows (2.5) , we can write the iteration procedure below

$$\begin{cases} t^k &= \mathbf{Dx^{k+1}} + \frac{\mathbf{w^k}}{\rho}, \\ \mathbf{z^{k+1}} &= \operatorname{prox}_{\mathbf{\Phi}_\gamma,\rho}(\mathbf{t^k}), \end{cases} \tag{3.12}$$

where $\operatorname{prox}_\Phi(\cdot)$ represents the proximal operator and it is useful in convex optimization, for more discussion, please see [52].

Now, we propose an iterative algorithm for solving the problem (3.9). Since the SCAD penalty function is used for the regular term in the model (3.9), we call this algorithm the SCADTV method (SCADTV).

Algorithm (SCADTV)

Step 0 *Initialization and date*:

Input parameters $\alpha \geq 0, \rho > 0, \lambda > 0, \gamma_1 > 0, \gamma_2 > 0$, the tolerance $\varepsilon > 0$. Given $(\mathbf{x}, \mathbf{z}, \mathbf{w}) := (\mathbf{x^0}, \mathbf{z^0}, \mathbf{w^0})$, let $k := 0$;

Step 1 Compute the new iterate $\widetilde{\mathbf{w}}^{\mathbf{k+1}} = (\mathbf{x^{k+1}}, \mathbf{z^{k+1}}, \mathbf{w^{k+1}})$ by (3.13);

$$\begin{cases} \mathbf{x^{k+1}} = (\mathbf{A^TA} + \rho\mathbf{D^TD})^{-1}\widehat{\mathbf{H}}_\mathbf{k}, \\ \mathbf{z^{k+1}} = \operatorname{prox}_{\mathbf{\Phi}_\gamma,\rho}(\mathbf{t^k}), \\ \mathbf{w}^{k+1} = \mathbf{w}^k - \rho(\mathbf{Dx^{k+1}} - \mathbf{z}^{k+1}). \end{cases} \tag{3.13}$$

Step 2 If $\|\widetilde{\mathbf{w}}^\mathbf{k} - \widetilde{\mathbf{w}}^{\mathbf{k+1}}\|_\mathbf{2}^\mathbf{2} \leq \varepsilon$, STOP; otherwise let $k =: k + 1$. Go back to step 1.

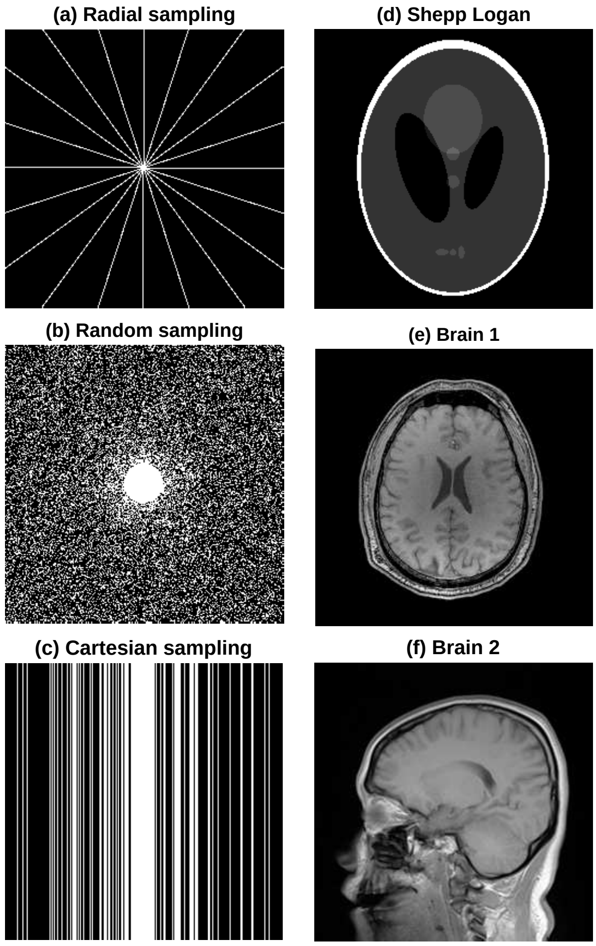

Fig. 2. Experimental datasets

4. Numerical results

In this section, we evaluate the performance of the proposed SCADTV method through some numerical experiments, and compare the proposed method with those of classic TV [40] and MCTV [23]. All of our test experiments are performed on MATLAB R2015a on the PC with Intel (R) Core (TM) 2.2 GHz CPU and and 8.0 GB RAM.

MRI test images recovery performance was evaluated by peak signal-to-noise ratio (PSNR) and relative error (RE), which are respectively defined as

$$\text{PSNR} = 10\lg\left(\frac{\mathbf{P}}{\|\mathbf{x}^k - \mathbf{x}\|_2^2}\right), \quad \text{RE} = \frac{\|\mathbf{x}^k - \mathbf{x}\|_2^2}{\|\mathbf{x}\|_2^2}.$$

where $\mathbf{x}$ is the original image, $\overline{\mathbf{x}}$ denotes the mean intensity value of $\mathbf{x}$, $\mathbf{x}^k$ is the restored image, $\mathbf{P}$ represents the size of the image. Usually, the larger PSNR value and the smaller RE value indicate better recovery performance.

The sampling templates and the test MR images are shown in Fig. 2: (a) is the radial sampling with 10 trajectory lines. (b) is the Random sampling with 30% sampling rate and 0.1 sampling radius. (c) is Cartesian under-sampling mask with a sampling rate of 34%. (d)-(f) are test images(sizes 256×256). (d) is Shepp Logan MRI data, (e) and (f) are two different of the brain MRI data images. More details can be found in [23], [49]. We set the parameters as: $\lambda = 0.01$, $\delta_1 = \delta_2 = 0.0001$, $\rho = 150$. The SCAD parameters were set $\gamma_2 = a\gamma_1$, $a = 3.7$. The optimized parameter γ_1 need to be set according to different sampling methods and data sets.

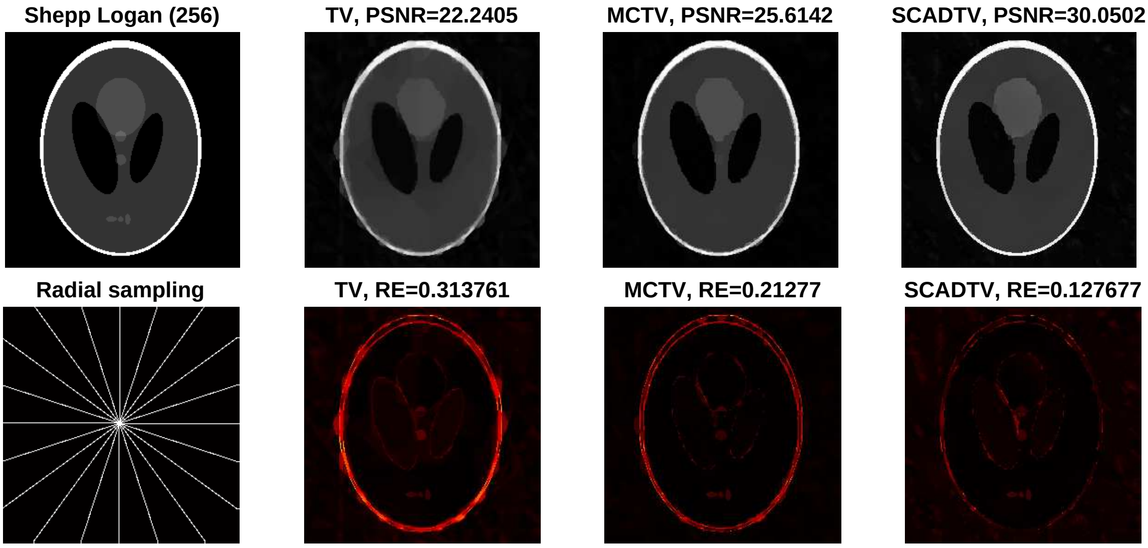

Fig. 3. Different reconstruction results of Shepp Logan (256) under radial sampling

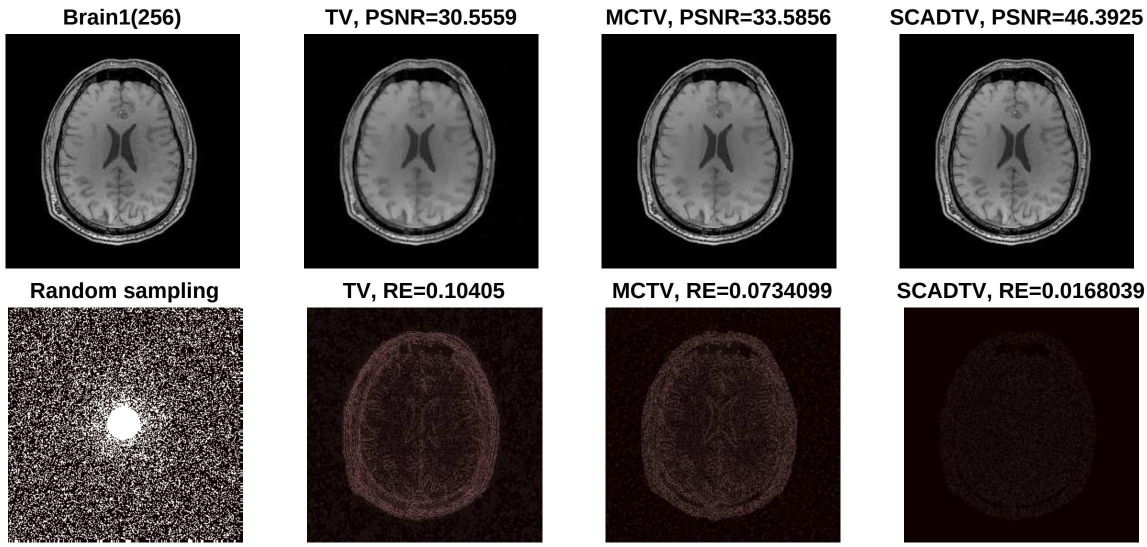

Fig. 4. Different reconstruction results of Brain1 (256) under random sampling

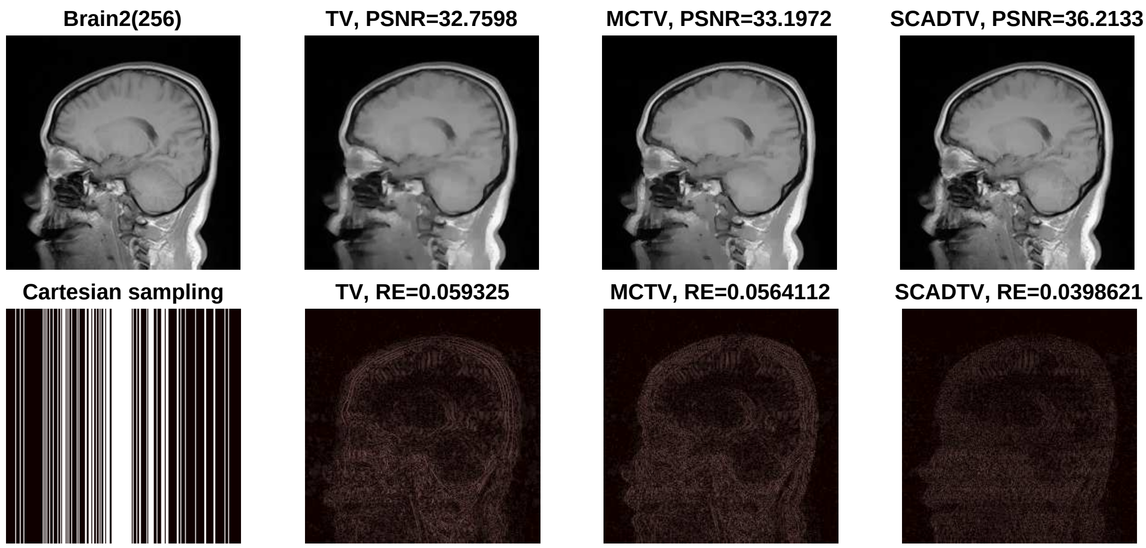

Fig. 5. Different reconstruction results of Brain2 (256) under cartesian sampling

TABLE I
THE VALUE OF PSN, RE AND CPUTIME UNDER DIFFERENT SAMPLING TEMPLATES.

Test Image	Template	Method	RE	PSNR(dB)	CPUtime(s)
Shepp Logan	Radial sampling	TV	0.3138	22.2405	2.805913
		MCTV	0.2128	25.6142	14.118701
		SCADTV	0.1277	30.0502	2.857253
Brain	Random sampling	TV	0.1041	30.5559	2.836221
		MCTV	0.0734	33.5856	15.004601
		SCADTV	0.0316	40.9066	2.968011
Brain2	Cartesian sampling	TV	0.0593	32.7598	2.951520
		MCTV	0.0564	33.1972	14.054279
		SCADTV	0.0399	36.2133	2.935640

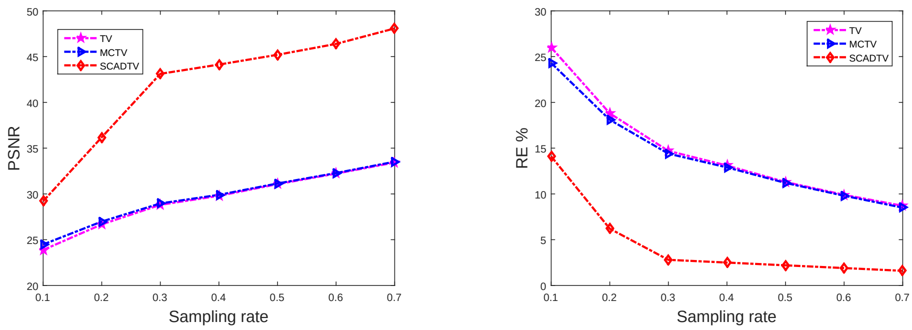

(a) Sampling rate VS PSRN (b) Sampling rate VS RE

Fig. 6. PSNR and RE versus sampling rate on Shepp Logan (256) with three reconstruction models under the radial sampling template

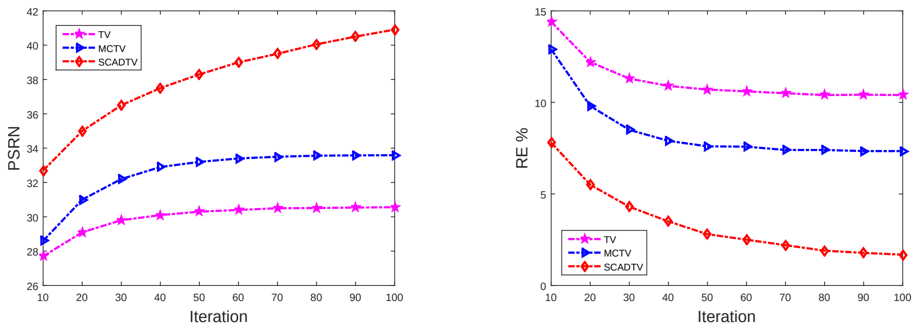

(a) Iteration VS PSRN (b) Iteration VS RE

Fig. 7. PSNR and RE versus Iteration on Brain1 (256) with three reconstruction models under the random sampling template with sampling rate of 30%.

The numerical experiments are divided into four parts. In the first part of the numerical experiment, we showed the reconstruction effects of different MRI test images and three sampling templates under different models. From Figs. 3-5, we can see the visual comparison of MRI reconstruction results under the different models.

In Fig. 3, Shepp Logan phantom is chosen to evaluate the performance of the proposed SCADTV model. We compare with the three reconstruction models (TV, MCTV, SCADTV) proposed above under the radial sampling template with 3.9% sampling rate. From the results, we can see that our SCADCTV method reconstructed Shepp Logan image with $PSNR \approx 30.05$, which higher TV, MCTV methods. That is to say, The performance of SCADTV is better than that of TV and MCTV. For the radial sampling results, the SCAD optimized parameter is set to ($\gamma_1 = 0.03$). For MR image Brain, we test the effectiveness of SCADTV method through the random sampling ($\gamma_1 = 0.001, \quad a = 100$). The reconstruction and error images are shown in Fig. 4. Because the Cartesian undersampling is k-space data, and is most widely used in practice. For Brain2, we test the image by using the Cartesian template mask under 0.34 sampling rate ($\gamma_1 = 0.01$). The reconstruction results were shown in Fig. 5. Through the visual comparison and analysis of the reconstruction results of three different methods shown in Figs. 3-5, it can conclude that the SCADTV always obtains better reconstruction results than the other two reconstruction models.

The reconstruction comparison results are shown in Table I. Compared with TV and MCTV, SCADTV method is more trustworthy and has better performance in testing MR images recovery, because it attained the higher PSNR and lower RE. From the table, we also know that SCADTV method needs about a fifth of the CPU time of MCTV in general. It is well know that appropriate selection of SCAD parameters are essential for its performance. For MRI data Brain 1, we test the reconstruction performances of SCADTV-model under the random sampling template with sampling rate of 30%. Our choice of $a = 3.7$ (or 50, 100, 200, 500) is based on the suggestion of the authors of [25] and [26]. Table II shows that the performance of SCADTV model is greatly affected by different parameters. According to the results in Table II, $\gamma_1 = 0.001, a = 100$ are considered to be the "best" choices SCAD parameters in this case. For more detailed discussion, please see [51].

The third part of the experiment, we compared MR image reconstruction performances at different sampling ratios and iterations. Fig. 6 show that for a fixed sampling ratio, the SCADTV method obtain higher PSNR and lower RE values than the mctv and TV. That is to say, the performances of SCADTV model are mostly better than MCTV and TV in this case. In addition, it is also know that the MCTV and TV achieve nearly the same values of PSNR and RE in this case. For a fixed iteration, Fig. 7 imply that the SCADTV performs mostly better than the MCTV and TV under the random sampling template with sampling rate of 30%.

Finally, we select two sets of 512×512 data to test the proposed method. In Fig. 8, the Shepp Logan data (512) were measured using a radial sampling template with 10 lines under 2% sampling rate. For Brain (512), cartesian sampling template with 15% sampling rate and random sampling template with 10% sampling rate was employed, respectively. Figs. 9-10 show clearly that the reconstruction result of SCAD method is superior than MCTV and TV methods.

TABLE II
RECONSTRUCTION RESULTS UNDER DIFFERENT VALUES OF SCAD PARAMETERS

Image	Template	SCAD parameters	RE	PSNR(dB)
Brain1(256)	Random sampling with 30%	$\gamma_1 = 0.0001, a = 3.7$	0.0305	41.2153
		$\gamma_1 = 0.001, a = 3.7$	0.0316	40.9066
		$\gamma_1 = 0.01, \quad a = 3.7$	0.0361	39.7594
		$\gamma_1 = 0.1, \quad a = 3.7$	0.1947	25.1145
		$\gamma_1 = 1, \quad a = 3.7$	0.8222	12.6009
Brain1(256)	Random sampling with 30%	$\gamma_1 = 0.0001, a = 50$	0.0305	41.2016
		$\gamma_1 = 0.001, a = 50$	0.0201	44.8514
		$\gamma_1 = 0.01, \quad a = 50$	0.0469	37.4706
		$\gamma_1 = 0.1, \quad a = 50$	0.2077	24.5516
		$\gamma_1 = 1, \quad a = 50$	0.8222	12.6008
Brain1(256)	Random sampling with 30%	$\gamma_1 = 0.0001, a = 100$	0.0304	41.2433
		$\boldsymbol{\gamma_1 = 0.001, a = 100}$	**0.0168**	**46.3925**
		$\gamma_1 = 0.01, \quad a = 100$	0.0505	36.8349
		$\gamma_1 = 0.1, \quad a = 100$	0.2081	24.5361
		$\gamma_1 = 1, \quad a = 100$	0.8222	12.6008
Brain1(256)	Random sampling with 30%	$\gamma_1 = 0.0001, a = 200$	0.0301	41.3338
		$\gamma_1 = 0.001, a = 200$	0.0171	46.2578
		$\gamma_1 = 0.01, \quad a = 200$	0.0525	36.4939
		$\gamma_1 = 0.1, \quad a = 200$	0.2082	24.5293
		$\gamma_1 = 1, \quad a = 200$	0.8222	12.6008
Brain1(256)	Random sampling with 30%	$\gamma_1 = 0.0001, a = 500$	0.0290	41.6427
		$\gamma_1 = 0.001, a = 500$	0.0191	45.2612
		$\gamma_1 = 0.01, \quad a = 500$	0.0538	36.2883
		$\gamma_1 = 0.1, \quad a = 500$	0.2085	24.5198
		$\gamma_1 = 1, \quad a = 500$	0.8222	12.6008

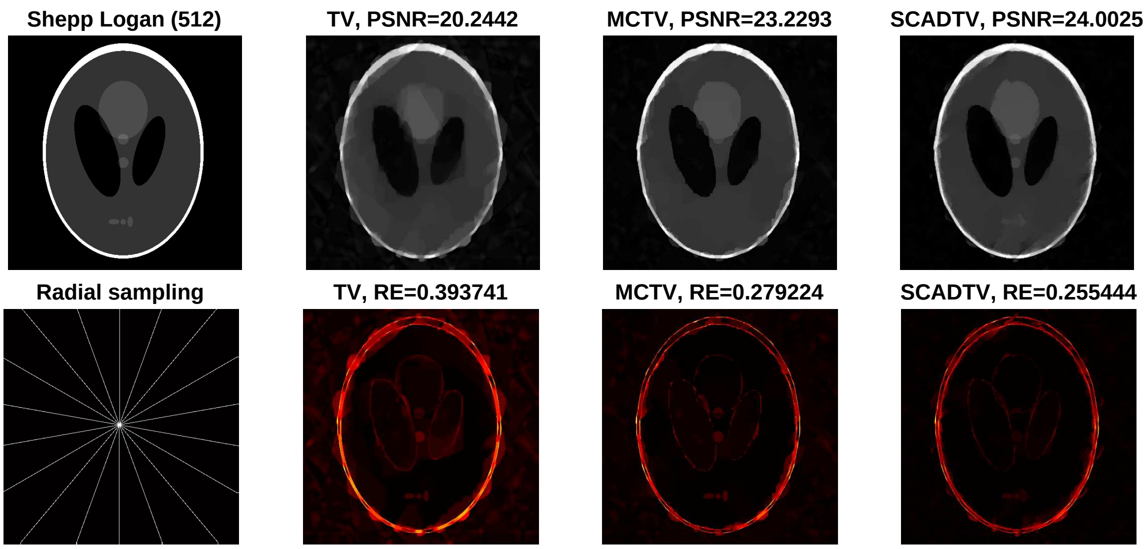

Fig. 8. Different reconstruction results of Shepp Logan (512) under radial sampling

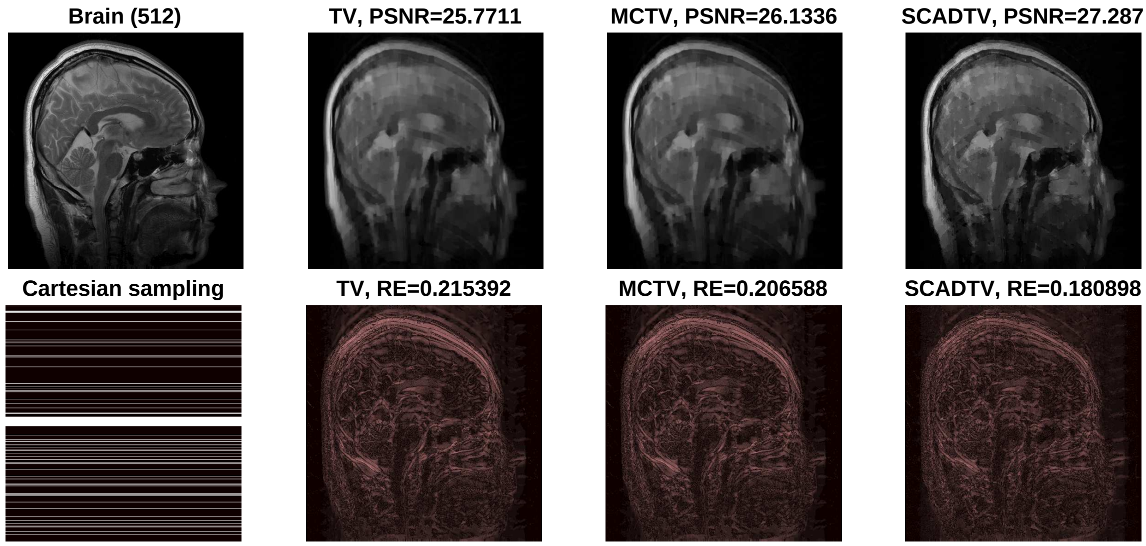

Fig. 9. Different reconstruction results of Brain (512) under cartesian sampling

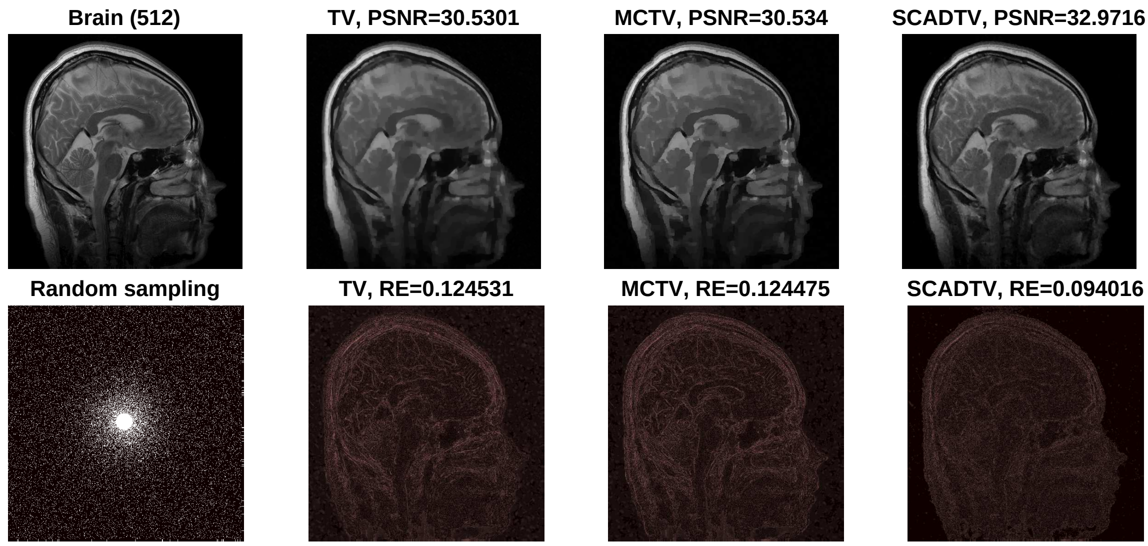

Fig. 10. Different reconstruction results of Brain (512) under random sampling

5. Conclusion

This work introduced a non-convex regularization model for MRI reconstruction via SCAD penalty function, which avoids the suboptimal local solutions and improves the fitting performance compared with the classical TV regularization. To solve this non-convex minimization problem, we use the ADMM method based on variable splitting technique, which can obtain some cheap closed-form solutions by proximal operator. Experimental results indicate that the SCADTV method proposed in this paper can significantly improve the MRI reconstruction effect. And the reconstructed MRI images show the superiority visual effects. In the future, this proposed method should be tested for more sparse systems such as dynamic magnetic resonance imaging etc.

Acknowledgment

The authors would like to thank Prof. Ivan Selesnick (http://eeweb.poly.edu/iselesni/index.html), Prof. Xiaobo Qu (https://csrc.xmu.edu.cn/index_cn/xiaobo/index_cn.html), and Junfeng Yang (https://math.nju.edu.cn/jfyang) for sharing the Datas, MATLAB codes and free download from their homepages.

References

[1] P. Mansfield, “Multi-planar image formation using NMR spin echoes,” *Journal of Physics C: Solid State Physics*, vol. 10, no. 3, pp. 55-58, 1977.

[2] A. Haase, J. Frahm, D. Matthaei, W. Hanicke, “Flash imaging rapid NMR imaging using low flip-angle pulses,” *Journal of Magnetic Resonance*, vol. 67, no. 2, pp. 258-266, 1986.

[3] M. Hutchinson and U. Raff, “Fast MRI data acquisition using multiple detectors,” *Magnetic Resonance in Medicine*, vol. 6, no. 1, pp. 87-91, 1988.

[4] D. Larkman and R. Nunes, “Parallel magnetic resonance imaging,” *Physics in Medicine & Biology*, vol. 52, no. 7, pp. 15-55, 2007.

[5] J. Hamilton, D. Franson and N. Seiberlich, “Recent advances in parallel imaging for MRI,” *Progress in Nuclear Magnetic Resonance Spectroscopy*, vol. 101, pp. 71-95, 2017.

[6] E. Candes, J. Romberg and T. Tao, “Robust uncertainty principles: exact signal reconstruction from highly incomplete frequency information,” *IEEE Transactions on Information Theory*, vol. 52, no. 2, pp. 489-509, 2006.

[7] M. Lustig, D. Donoho and J. Pauly, “Sparse MRI: The application of compressed sensing for rapid MR imaging,” *Magnetic Resonance in Medicine*, vol. 58, no. 6, pp. 1182-1195, 2007.

[8] M. Lustig, D. Donoho, J. Santos, et al, “Compressed sensing MRI,” *IEEE Signal Processing Magazine*, vol. 25, no. 2, pp. 72-82, 2008.

[9] R. Chartrand and V. Staneva, "Restricted isometry properties and nonconvex compressive sensing," *Inverse Problems*, vol. 24, no. 3, pp. 035020, 2008.

[10] J. Haldar and J. Zhuo, "P-Loraks: Low-rank modeling of local k-space neighborhoods with parallel imaging data," *Magnetic Resonance in Medicine*, vol. 75, no. 4, pp. 1499-1514, 2016.

[11] J. He, Q. Liu, A. Christodoulou, et al, "Accelerated high-dimensional MR imaging with sparse sampling using low-rank tensors," *IEEE Transactions on Medical Imaging*, vol. 35, no. 9, pp. 2119-2129, 2016.

[12] Y. Hu, X. Liu and M. Jacob, "A generalized structured low-rank matrix completion algorithm for MR image recovery," *IEEE Transactions on Medical Imaging*, vol. 38, no. 8, pp. 1841-1851, 2019.

[13] W. Chan and K. Sim, "Termination factor for iterative noise reduction in MRI images using histograms of second-order derivatives," *IAENG International Journal of Computer Science,* vol. 48, no. 1, pp. 174-180, 2021.

[14] M. Doneva, "Mathematical models for magnetic resonance imaging reconstruction: an overview of the approaches, problems, and future research areas," *IEEE Signal Processing Magazine*, vol. 37, no. 1, pp. 24-32, 2020.

[15] J. Cands, M. Wakin and S. Boyd, "Enhancing sparsity by reweighted ℓ_1 minimization," *Journal of Fourier Analysis and Applications,* vol. 14, pp. 877-905, 2008.

[16] S. Foucart and M. Lai, "Sparsest solutions of underdetermined linear systems via ℓ_q-minimization for $0 < q \leq 1$," *Applied and Computational Harmonic Analysis*, vol. 26, no. 3, pp. 395-407, 2009.

[17] I. Daubechies, R. Devore, M. Fornasier, et al, "Iteratively reweighted least squares minimization for sparse recovery," *Communications on Pure and Applied Mathematics,* vol. 63, no. 1, pp. 1-38, 2010.

[18] M. Lai, Y. Xu and W. Yin, "Improved iteratively reweighted least squares for unconstrained smoothed ℓ_q minimization," *SIAM Journal on Numerical Analysis*, vol. 51, no. 2, pp. 927-957, 2013.

[19] Pant J, Lu W, Antoniou A, et al. "New improved algorithms for compressive sensing based on ℓ_p norm," *IEEE Transactions on Circuits and Systems Ii-express Briefs*, vol.61, no.3, pp198-202, 2014.

[20] F. Wen, L. Chu, P. Liu, et al, "A survey on nonconvex regularization-based sparse and low-rank recovery in signal processing, statistics, and machine learning," *IEEE Access*, vol. 6, pp. 69883-69906, 2018.

[21] I. Selesnick, "Sparse regularization via convex analysis," *IEEE Transactions on Signal Processing*, vol. 65, no. 17, pp. 4481-4494, 2017.

[22] I. Selesnick, A. Lanza, S. Morigi, et al, "Non-convex total variation regularization for convex denoising of signals," *Journal of Mathematical Imaging and Vision*, vol. 62, pp. 825-841, 2020.

[23] Y. Liu, H. Du, Z. Wang, et al, "Convex MR brain image reconstruction via non-convex total variation minimization," *International Journal of Imaging Systems and Technology*, vol. 28, no. 4, pp. 246-253, 2018.

[24] M. Shen, J. Li, T. Zhang and J. Zou, "Magnetic resonance imaging reconstructionvia non-convex total variation regularization," *International Journal of Imaging Systems and Technology*, pp. 1-13, Jul. 2020.

[25] J. Fan and R. Li, "Variable selection via nonconcave penalized likelihood and its oracle properties," *Journal of the American Statistical Association*, vol. 96, no. 456, pp. 1348-1360, 2001.

[26] A. Mehranian, H. Rad, A. Rahmim, et al, "Smoothly clipped absolute deviation (SCAD) regularization for compressed sensing MRI using an augmented Lagrangian scheme," *Magnetic Resonance Imaging*, vol. 31, no. 8, pp. 1399-1411, 2013.

[27] L. Chen, D. Wei and J. Wang, "Research on magnetic resonance imaging segmentation algorithm," *Engineering Letters,* vol. 27, no. 3, pp. 559-567, 2019.

[28] S. Ramani, and J. Fessler, "Parallel MR image reconstruction using augmented Lagrangian methods," *IEEE Transactions on Medical Imaging*, vol. 30, no. 3, pp. 694-706, 2011.

[29] J. Aelterman, H. Luong, B. Goossens, et al, "Augmented Lagrangian based reconstruction of non-uniformly sub-Nyquist sampled MRI data," *Signal processing*, vol. 91, no. 12, pp. 2731-2742, 2011.

[30] Y. Lian , J. Zhou, et al, "On the existence of saddle points for ℓ_1-Minimization problems," *IAENG International Journal of Applied Mathematics*, vol. 51, no. 1, pp. 48-56, 2021.

[31] A. Chambolle and T. Pock, "A first-order primal-dual algorithm for convex problems with applications to imaging," *Journal of Mathematical Imaging and Vision*, vol. 40, no. 1, pp. 120-145, 2011.

[32] Y. Chen, W. Hager, F. Huang, et al, "Fast algorithms for image reconstruction with application to partially parallel MR imaging," *SIAM Journal on Imaging Sciences*, vol. 5, no. 1, pp. 90-118, 2012.

[33] X. Ye, Y. Chen and F. Huang, "Computational acceleration for MR image reconstruction in partially parallel imaging," *IEEE transactions on medical imaging*, vol. 30, no. 5, pp. 1055-1063, 2011.

[34] Y. Zhu and Y. Shi, "A fast method for reconstruction of total-variation MR images with a periodic boundary condition," *IEEE signal processing letters*, vol. 20, no. 4, pp. 291-294, 2013.

[35] J. Duan, Y. Liu and L. Zhang, "Bregman iteration based efficient algorithm for MR image reconstruction from undersampled K-space data," *IEEE Signal Processing Letters*, vol. 20, no. 8, pp. 831-834, 2013.

[36] A. Beck and M. Teboulle, " A fast iterative shrinkage-thresholding algorithm for linear inverse problems," *SIAM Journal on Imaging sciences*, vol. 2, no. 1, pp. 183-202, 2009.

[37] I. Daubechies, M. Defrise and C. De Mol, "An iterative thresholding algorithm for linear inverse problems with a sparsity constraint," *communications on pure & applied mathematics*, vol. 57, no. 11, pp. 1413-1457, 2003.

[38] D. Cristhian, M. Molina-Machado, D. Juan, V. Martinez and Eduardo Giraldo, "Large sparse state estimation based on a parallel dual adaptive FISTA method," *Engineering Letters*, vol. 28, no. 4, pp. 985-990, 2020.

[39] S. Pejoski, V. Kafedziski and D. Gleich, "Compressed sensing MRI using discrete nonseparable shearlet transform and FISTA," *IEEE Signal Processing Letters*, vol. 22, no. 10, pp. 1566-1570, 2015.

[40] J. Yang, Y. Zhang and W. Yin, "A fast alternating direction method for TVL1-L2 signal reconstruction from partial fourier data," *IEEE Journal of Selected Topics in Signal Processing*, vol. 4, no. 2, pp. 288-297, 2010.

[41] Y. Yan, H. Li, Z. Xu, et al, "Deep ADMM-Net for compressive sensing MRI," *Advances in Neural Information Processing Systems*, Spain, pp. 10-18, 2016.

[42] B. Zhang and Z. Zhu, "Linearized proximal alternating direction method of multipliers for parallel magnetic resonance imaging," *IEEE/CAA Journal of Automatica Sinica*, vol. 4, no. 4, pp. 763-769, 2017.

[43] M. Le and J. Fessler, "Efficient, convergent sense MRI reconstruction for nonperiodic boundary conditions via tridiagonal solvers," *IEEE Transactions on Computational Imaging,* vol. 3, no. 1, pp. 11-21, 2017.

[44] B. He, F. Ma and X. Yuan, "Optimal proximal augmented Lagrangian method and its application to full Jacobian splitting for multi-block separable convex minimization problems," *IMA Journal of Numerical Analysis*, vol. 40, pp. 1188-1216, 2020.

[45] J. Cui, G. Peng, Q. Lu, et al, "Special regularized HSS iteration method for Tikhonov regularization," *IAENG International Journal of Applied Mathematics*, vol. 50, no. 2, pp. 359-372, 2020.

[46] C. Lin and J. Fessler, "Efficient dynamic parallel MRI reconstruction for the low-rank plus sparse model," *IEEE Transactions on Computational Imaging*, vol. 5, no. 1, pp. 17-26, 2018.

[47] J. Fessler, "Optimization methods for magnetic resonance image reconstruction: key models and optimization algorithms," *IEEE Signal Processing Magazine*, vol. 37, no. 1, pp. 33-40, 2020.

[48] S. Boyd, N. Parikh, E. Chu, et al, "Distributed optimization and statistical learning via the alternating direction method of multipliers," *Foundations and Trends in Machine Learning*, vol. 3, no. 1, pp. 1-122, 2011.

[49] Y. Liu, Z. Zhan, J. Cai, et al, "Projected iterative soft-thresholding algorithm for tight frames in compressed sensing magnetic resonance imaging," *IEEE Transactions on Medical Imaging*, vol. 35, no. 9, pp. 2130-2140, 2016.

[50] Y. Wang, W. Yin and J. Zeng, "Global convergence of ADMM in nonconvex nonsmooth optimization," *Journal of Scientific Computing*, vol. 78, no. 7, pp. 29-63, 2019.

[51] G. Gu, J. Jiang and J. Yang, "A TVSCAD approach for image deblurring with impulsive noise," *Inverse Problems*, vol. 33, no. 12, pp. 125008, 2017.

[52] H. Bauschke and P. Combettes, "Convex analysis and monotone Operator theory in hilbert spaces 2nd ed," Springer, New York, 2017.